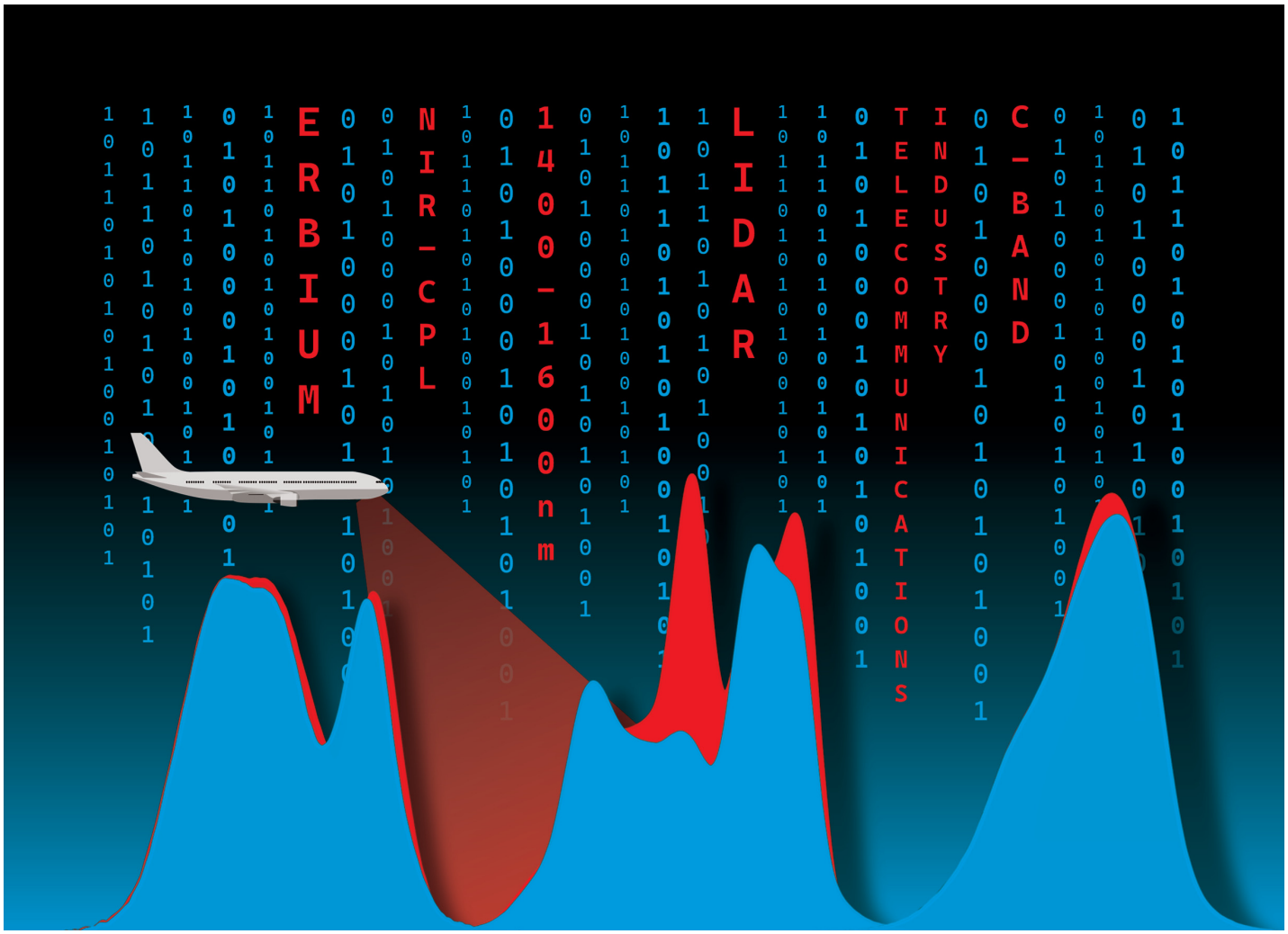

Showcasing research from Professor Lorenzo Di Bari's laboratory, Dipartimento di Chimica e Chimica Industriale, Università di Pisa, Pisa, Italy.

Intense 1400–1600 nm circularly polarised luminescence from homo- and heteroleptic chiral erbium complexes

Near infrared (NIR) circularly polarized luminescence (CPL) was measured for several chiral erbium complexes between 1400 to 1600 nm. The strong CPL and wavelength region have potential applications from biology to the telecommunications industry.

As featured in:

See Francesco Zinna, Lorenzo Di Bari *et al.*, *J. Mater. Chem. C*, 2023, **11**, 5290.

ROYAL SOCIETY OF CHEMISTRY

rsc.li/materials-c

Registered charity number: 207890

Journal of Materials Chemistry C

ROYAL SOCIETY OF CHEMISTRY

PAPER

View Article Online
View Journal | View Issue

Cite this: J. Mater. Chem. C, 2023, 11, 5290

Intense 1400–1600 nm circularly polarised luminescence from homo- and heteroleptic chiral erbium complexes†

Oliver G. Willis, [a] Andrea Pucci, [a] Enrico Cavalli, [b] Francesco Zinna *[a] and Lorenzo Di Bari *[a]

Received 3rd January 2023,
Accepted 12th March 2023

DOI: 10.1039/d3tc00034f

rsc.li/materials-c

Efficient near-infrared circularly polarised luminescence (CPL) between 1400 and 1600 nm of four enantiomer pairs of homo- and heteroleptic complexes has been successfully measured. Utilising inexpensive optics and a commercial fluorimeter, discrimination of the left and right circularly polarised components was achieved, yielding remarkably high dissymmetry values in emission (g_{lum}). Most notably, homoleptic complexes $CsEr(hfbc)_4$ (hfbc = 3-heptafluorobutylyrylcamphorate) and $[TMG{-}H^+]_3Er(BINOLate)_3$ (TMG = 1,1,3,3-tetramethylguanidine; BINOLate = 1,1′-bi-2-naphtholate) show maximal $|g_{lum}|$ values of 0.83 (at 1510 nm) and 0.29 (at 1545 nm) respectively, with the former complex possessing the strongest CPL within the NIR to date.

Introduction

Chiral lanthanide complexes, in recent years, have shown interesting and unique optical and chiroptical properties,[1–16] which have made their use within the context of chiral electronics and photonics highly desirable. In general, compounds with substantial optical activity have already shown their importance in current technologies such as circularly polarised OLEDs,[17–19] polarisation-sensitive phototransistors[20] and spin filters.[21] In particular, lanthanide chiral complexes may feature narrow emission bands, large pseudo-Stokes shifts, long lifetimes, strong circular dichroism (CD) and circularly polarised luminescence (CPL). Chiral lanthanide complexes which show strong CPL within the visible region have already been successfully employed in (bio)-assays[22–24] and within circularly polarised OLEDs.[17,25] Unlike the emission of most organic systems, the f–f transitions are not only limited to the visible region, and indeed span a wide spectral range into the near-infrared (NIR). Species which emit within the NIR and show significant chiroptical properties have potential uses ranging from biological applications[2,26] to the telecommunications industry. Indeed, Erbium, which emits around 1530 nm, is used as a dopant in current LASER systems, which are involved in the free-space long-distance optical transmission or fibre optical communications (the so-called C-band).[27,28] Besides applications of NIR luminescence in general, few reports describe CPL of Yb-based systems which emit *ca.* 1000 nm.[29–34] Even more rare are reports of NIR-CPL in the 1400–1600 nm range, achievable with chiral Er complexes, with only two occurrences to date, both published in 2022.[1,3] This is likely due to the fact that instrumentation with capabilities of measuring lower energy NIR-CPL is not readily available, which in turn slows down the development of NIR-CPL active molecular compounds. In the current state of the art, it is therefore of significant interest to expand the scope of NIR-CPL active compounds to open the way to applications in chiral electronic device CPL microscopy, *etc.*

This work aims to show how with a simple setup, Er NIR-CPL between 1400 and 1600 nm can be measured even with easily accessible Er complexes, which are not necessarily designed for the purpose of sensitising the low energy emission.[1]

We also emphasise the interesting chiroptical features of the $^4I_{15/2} \rightarrow {}^4I_{13/2}$ transition of Er, which was predicted to show strong optical and chiroptical properties by Richardson in 1980.[35] The $^4I_{15/2} \rightarrow {}^4I_{13/2}$ transition of Er belongs within classes EI (electric dipole strength), RI (rotatory strength) and DII (dissymmetry factor), which should show relatively favourable optical and chiroptical properties compared to other lanthanide transitions.[35] From our previous work, we showed that this prediction is indeed valid, and that transitions belonging to such classes do show remarkably strong NIR chiroptical properties.[2]

Thanks to chiral lanthanide complexes possessing extraordinarily high dissymmetry factors, compared to other chiral isolated molecules (*i.e.*, non-aggregated systems),[36–40] we were

[a] Dipartimento di Chimica e Chimica Industriale, Università di Pisa, via Moruzzi 13, Pisa 56124, Italy. E-mail: francesco.zinna@unipi.it, lorenzo.dibari@unipi.it
[b] Department of Chemical Sciences, Life and Environmental Sustainability, University of Parma, Parco Area delle Scienze 11/a, 43124, Parma, Italy

† Electronic supplementary information (ESI) available: Compound preparation, instrumentation details and additional spectra. See DOI: https://doi.org/10.1039/d3tc00034f

able to utilise a basic setup which requires inexpensive optical components and simple 3D-printed holders (Fig. S1, ESI†) to discriminate the circularly polarised components of the luminescence (Fig. S8, S14 and S20, ESI†).[1] A standard commercial fluorimeter equipped with a liquid nitrogen-cooled InGaAs detector was used to collect the Er NIR emission, and the circular polarisation discrimination was achieved by 90° rotation of the quarter-wave plate (QWP), preceding a linear polariser (LP), whose axes were reciprocally oriented at ± 45° (See ESI† for more details).[1]

In order to show that Er CPL can be observed from a variety of structures, four enantiomer pairs of chiral Er complexes were studied, two homoleptic and two heteroleptic systems, belonging to different classes of symmetry (C_4, D_3 and C_1). The two homoleptic complexes were $CsEr(hfbc)_4$ (hfbc = 3-heptafluorobutylyrylcamphorate) and $[TMG{-}H^+]_3Er(BINOLate)_3$ (TMG = 1,1,3,3-tetramethylguanidine; BINOLate = 1,1′-bi-2-naphtholate) shown in Scheme 1. The former complex scaffold has been well studied across the series of lanthanides in regard to its structure in solution and chiroptical properties.[2,12,41–43] The Eu and Yb complexes uphold the current highest $|g_{lum}|$ in both the visible (1.38 at 595 nm)[12,42] and NIR (0.38 at 988 nm),[2] respectively. Such complexes have an antiprismatic coordination geometry, which is ideal for an efficient dynamic coupling, through which the lanthanide f–f transitions can gain sizeable rotatory strength from ligand-centred transitions.[43] The latter complex, $[TMG{-}H^+]_3Er(BINOLate)_3$, is the air- and water-stable analogue[44] of Shibasaki's rare earth alkali metal BINOLate (REMB), pinwheel-shaped complex.[45] The original Er Shibasaki complex was recently reported to show NIR-CPL at *ca.* 1550 nm.[3] In our previous work, we noted that the exchange of the alkali earth metal in the REMB complex with the organic tetra methyl guanidinium[44] causes a structural rearrangement of the binaphthol ligands around the lanthanide, while still retaining an overall D_3 solution geometry.[2] The reorganisation of the binaphthol moieties is due to a change in the coordination polyhedron from a distorted trigonal antiprism geometry of the Shibasaki analogue[3,4,46] to a distorted octahedron.[2,3,44] This change is a result of the stereogenic axis rotating away from being almost parallel to the C_3 principal axis, while both structures retain similar bite angles. The two heteroleptic complexes are formed by diketonate-based ligands as sensitisers of Er emission and the commercially available pyridine bis(oxazoline) derivatives as the chirality-inducing component. This allows one to tune independently the overall emission efficiency and CPL intensity. For this study, 4,4,4-trifluoro-1-(2-naphthyl)-1,3-butanedionate (NTA) acted as the Er sensitiser,[47] while 2,6-bis(4-isopropyl-2-oxazolin-2-yl)pyridine (*i*PrPyBox) and 2,6-bis(4-phenyl-2-oxazolinyl)pyridine (PhPyBox) were used to provide the necessary chiral environment (Scheme 1). Similar strategies were reported for Yb and Eu CPL-active complexes.[25,26,48–50] A direct correlation between structure and CPL properties remains elusive for lanthanide complexes in the current state of the art. Nevertheless, a few qualitative insights can be gained on the role played by the complex geometry in the case of Er CPL.

Results and discussion

$CsEr(hfbc)_4$

In THF, the $CsEr(hfbc)_4$ complex shows a UV-Vis absorption centred at 310 nm with a shoulder at lower energy (Fig. S4, ESI†). The excitation profile traces the low-energy shoulder with the maximum at 325 nm (Fig. S4, ESI†). Upon excitation, a structured emission profile is observed, containing a minimum of four distinct maxima occurring at 1477, 1509, 1530 and 1542 nm (Fig. 1). Each maximum is seemingly associated to a corresponding CPL signal, which are equal and opposite for the two enantiomers (Fig. 1). From high to low energy, the four

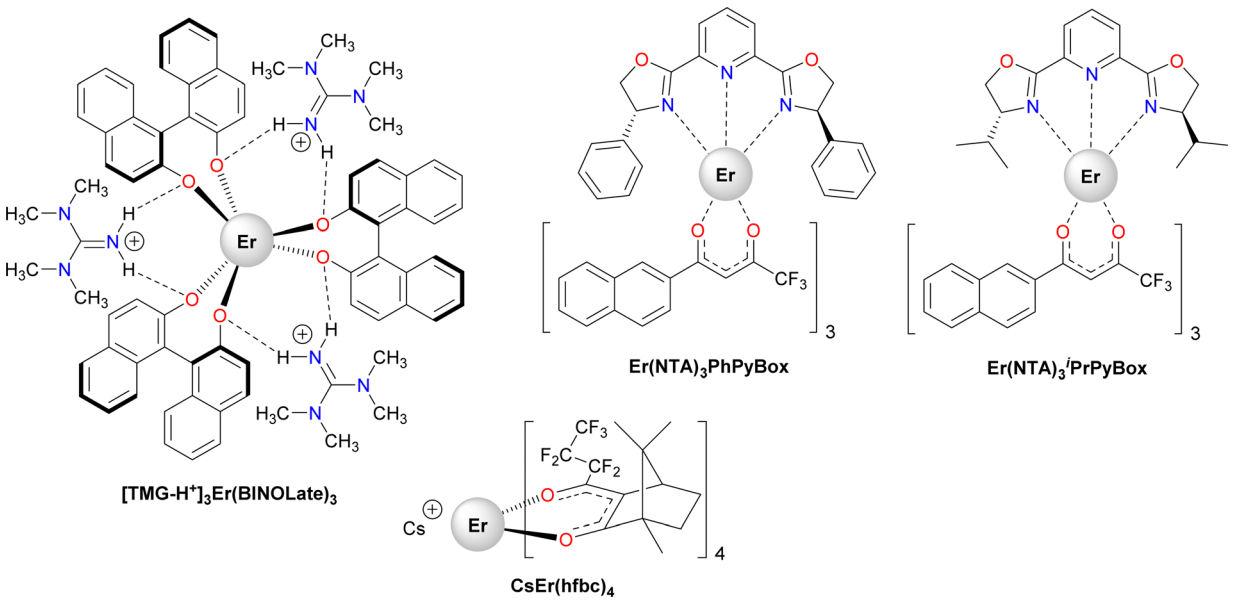

Scheme 1 Structures of the four enantiomer pairs of complexes studied in this work.

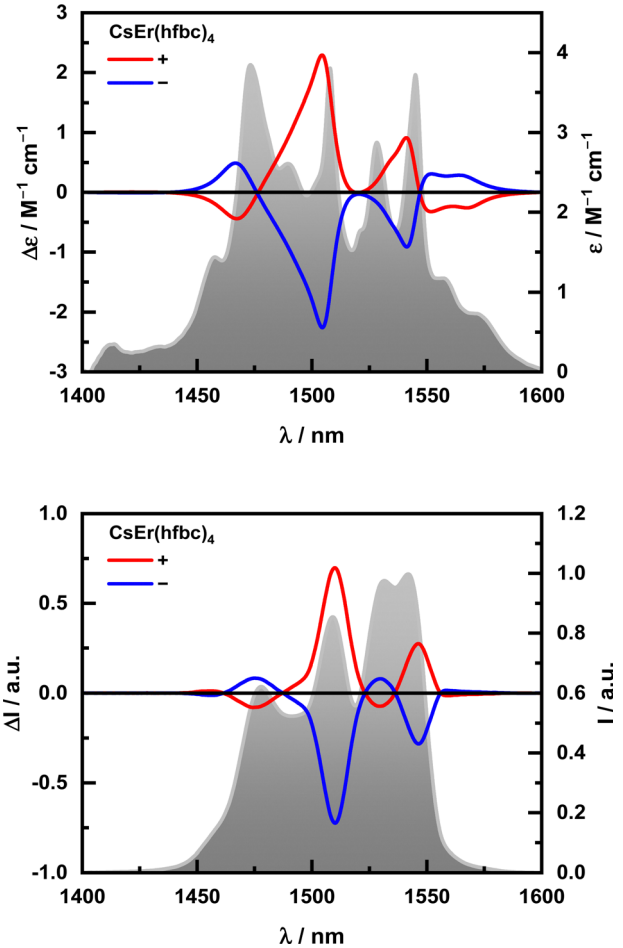

Fig. 1 (Top) NIR-CD spectra of $CsEr(hfbc)_4$ (16 mM) with average total absorption traced in the background (in grey). (Bottom) NIR-CPL spectra of $CsEr(hfbc)_4$ (1 mM) with normalised average total emission traced in the background (in grey, λ_{ex} = 325 nm). Both spectra were recorded in anhydrous THF at room temperature.

predominant CPL signals have an alternating sign, *e.g.* −/+/−/+ for (+)-$CsEr(hfbc)_4$ and *vice-versa* for (−)-$CsEr(hfbc)_4$. The four distinct $|g_{lum}|$ maxima occur at 1472, 1510, 1530, and 1550 with corresponding values of 0.15, 0.83, 0.08 and 0.38 (Fig. S7, ESI†). We recall that $CsEr(hfbc)_4$ features a C_4-symmetric structure, with an achiral coordination polyhedron, where lanthanide f–f transitions may gain rotatory strength only through coupling with ligand-centered transitions (dynamic coupling).[43] Such high values of g_{lum} confirm the effectiveness of the dynamic coupling mechanism even in cases where ligand and lanthanide- transitions are extremely distant in energy (approximately 25 500 cm^{-1}, in the present case).

The NIR-CD spectrum shows a similar sign pattern and shape as the NIR-CPL, except for the absence of a CD band at *ca.* 1530 nm (Fig. S6, ESI†). The NIR absorption spectrum shows multiple narrow emission bands of varying transition dipole intensities (Fig. 1). The main CD bands occur at 1566, 1505, 1540, 1553 and 1565 nm with corresponding $|g_{abs}|$ values of 0.27, 0.91, 0.40, 0.26 and 0.36 (Fig. S7, ESI†). Comparing these values to those previously reported for the same complex, measured in $CDCl_3$ rather than THF, we see almost identical chiroptical features, suggesting that the solvent has little impact on the structural arrangement of the ligands and electronic properties of the complex. This confirms the stability of the *tetrakis* structure in solution, determined by the interaction of the perfluorinated chains with Cs^+ cation.[43] The liquid N_2 cooled InGaAs detector used for measuring the NIR emission and CPL has a sharp decrease in efficiency after 1550 nm and therefore, possible transitions present at lower energies are not observed (Fig. S4, ESI†). Anyway, this cut-off has no impact on the g_{lum} values reported. The $CsEr(hfbc)_4$ complex shows an overall quantum yield (Q_L^{Er}) of 0.004%, measured using $Yb(TTA)_3(H_2O)_2$ (TTA = thenoyltrifluoroacetone, Q_L^{Yb} = 0.35% in toluene)[51] as the reference. Despite the poor quantum yield, reliable and reproducible NIR-CPL can be measured.

$[TMG{-}H^+]_3Er(BINOLate)_3$

The D_3-symmetric, binaphtholate-based homoleptic complex $[TMG{-}H^+]_3Er(BINOLate)_3$ shows extremely rich chiroptical features, similar to the previously discussed $CsEr(hfbc)_4$. Upon ligand excitation at 365 nm (Fig. S10, ESI†), a weak emission profile consisting of a minimum of three major bands was observed (Fig. 2). Despite the low emission intensity, the CPL was easily measured due to the complex high dissymmetry factors (Fig. 2). The three low-energy major CPL bands of alternating sign at 1515, 1526 and 1545 nm give $|g_{lum}|$ values of 0.13, 0.23 and 0.29, respectively (Fig. S13, ESI†). The high-energy CPL band shows a $|g_{lum}|$ of 0.11 at 1455 nm. As introduced earlier, the NIR-CPL of the original Shibasaki scaffold with Er has been measured previously. Although both complexes possess the same D_3 solution geometry, the structural rearrangement of the binaphtholate moieties leads to a significant change in chiroptical features. Ung *et al.* observed two dominant emission bands at 1470 and 1540 nm, like those reported here (Fig. 2) with the predominant chiroptical activity arising from the latter. Unlike the CPL reported by Ung, which shows a large monosignate band at 1540 nm, we measure up to three relatively intense bands of alternating sign (*vide supra*). Despite these changes, both complexes display similar dissymmetry factors.[3] The $[TMG{-}H^+]_3Er(BINOLate)_3$ complex also exhibits an extremely short lifetime of *ca.* 0.4 μs (Fig. S15, ESI†).

As with the $CsEr(hfbc)_4$ complex, both the NIR-CD and NIR-CPL show remarkable similarity in terms of sign and shape, with a slightly different maxima offset (Fig. S12, ESI†). The NIR-CD shows an additional intense signal at 1554 nm (Fig. 2) which corresponds to the highest $|g_{abs}|$ (0.71) in the entire spectra. This signal is partially lost in the NIR-CPL due to the detector cut-off (Fig. S3, ESI†). The four remaining intense CD bands at 1457, 1508, 1520 and 1537 nm show dissymmetry values of 0.17, 0.12, 0.43 and 0.24, respectively (Fig. S13, ESI†).

$Er(NTA)_3$*i*Pr/PhPyBox

Both the C_1-symmetric $Er(NTA)_3$*i*PrPyBox and $Er(NTA)_3$PhPyBox contain the sensitising ligand, NTA, which possesses a strong electronic transition centred around 345 nm (Fig. S16 and S22, ESI†). Upon excitation, both complexes show a single, narrow emission band with a small shoulder at higher energy (Fig. 3

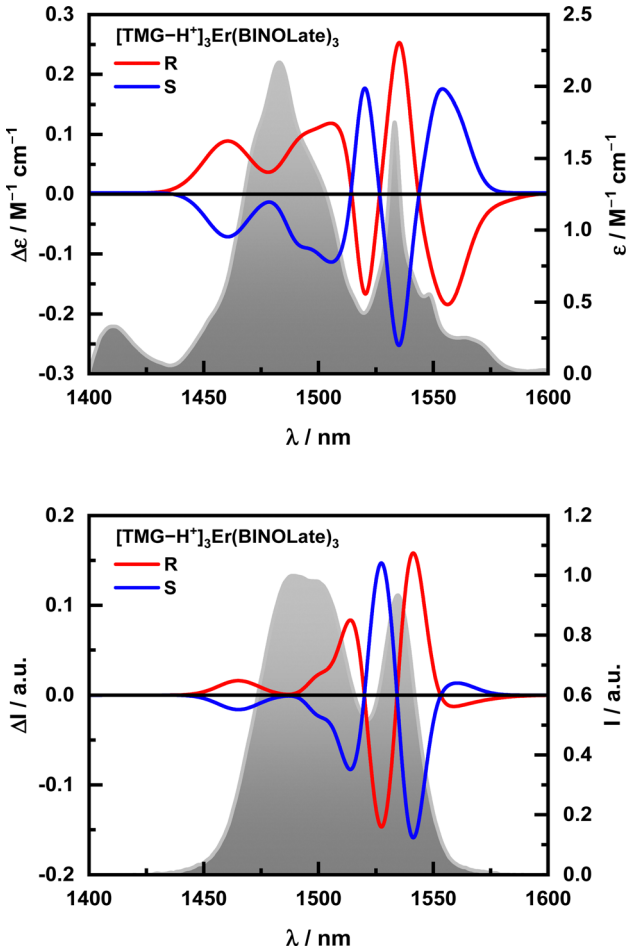

Fig. 2 (Top) NIR-CD spectra of $[TMG{-}H^+]_3Er(BINOLate)_3$ (26 mM) with average total absorption traced in the background (in grey). (Bottom) NIR-CPL spectra $[TMG{-}H^+]_3Er(BINOLate)_3$ (1 mM) with normalised average total emission traced in the background (in grey, λ_{ex} = 365 nm). Both spectra were recorded in anhydrous THF at room temperature.

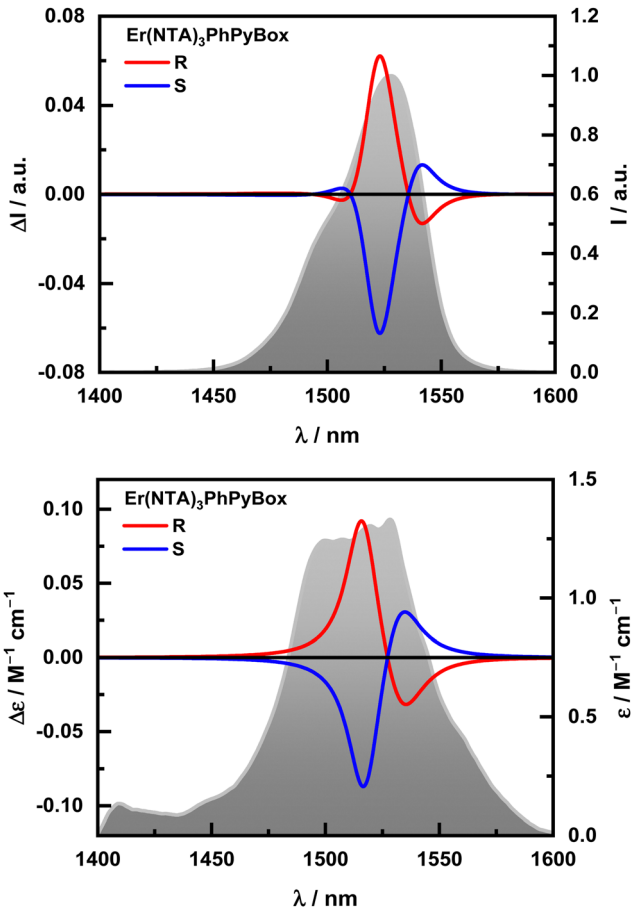

Fig. 3 (Top) NIR-CD spectra of $Er(NTA)_3PhPyBox$ (37 mM) with average total absorption traced in the background (in grey). (Bottom) NIR-CPL spectra of $Er(NTA)_3PhPyBox$ (1 mM) with normalised average total emission traced in the background (in grey, λ_{ex} = 345 nm). Both spectra were recorded in anhydrous THF at room temperature.

and Fig. S16 and S22, ESI†). $Er(NTA)_3PhPyBox$ shows simple chiroptical features in both NIR absorption and emission compared to the previous homoleptic Er complexes (Fig. 3). The similarity between the NIR-CD and NIR-CPL is again apparent (Fig. S18, ESI†). The NIR-CD spectrum shows only two major bands of opposite sign occurring at 1516 and 1535 nm with corresponding $|g_{abs}|$ of 0.07 and 0.03 (Fig. S19, ESI†). The NIR-CPL shows a similar bisignate signal with maxima at 1523 and 1542 nm with $|g_{lum}|$ values of 0.06 and 0.02 (Fig. S19, ESI†).

Unlike $Er(NTA)_3PhPyBox$, the $Er(NTA)_3iPrPyBox$ complex shows no measurable chiroptical activity neither in absorption nor emission. This behaviour is related to the different geometry of the complexes in the two cases. Indeed, the ECD spectra (Fig. S16 and S22, ESI†) show an exciton couplet associated to the diketonate-centred π–π* transition. The couplet crossover is at 355 nm in the case of $Er(NTA)_3iPrPyBox$, while it is blue shifted for $Er(NTA)_3PhPyBox$ by approximately 15 nm. This indicates a different skew angle between the NTA ligands in $Er(NTA)_3iPrPyBox/PhPyBox$ complexes. The photophysical properties for both $Er(NTA)_3iPrPyBox$ and $Er(NTA)_3PhPyBox$ were measured and showed similar characteristics. Both complexes showed an overall quantum yield of 0.003% and lifetimes of 2.7 μs (Fig. S21 and S24, ESI†). Interestingly the simple change of the substituents of the chiral ancillary ligands has an enormous impact on the chiroptical properties of the complex, while it has no significant effect on the emission properties (see Table 1). This corroborates the idea that in such heteroleptic compounds, chiroptical and photophysical properties can be optimized rather independently.[25]

With overall quantum yields and emission lifetimes values in hand (Table 1), it is possible to extract valuable information about the photophysical processes involved in the emission. $CsEr(hfbc)_4$ shows an excited state lifetime (τ_{obs}) of 6.6 μs (Fig. S9, ESI†), significantly higher than commonly reported (optically inactive) Er compounds.[47,52,53] Assuming a radiative lifetime (τ_{rad}) of 10 ms from the literature,[52–54] an internal quantum yield ($Q_{Er}^{Er} = \tau_{obs}/\tau_{rad}$) of 0.07% can be calculated, as well as a sensitisation efficiency ($\eta_{sens} = Q_L^{Er}/Q_{Er}^{Er}$) of approximately 6%. These values may be compared to the sensitisation efficiency of 75%, and an approximately 10-times higher Q_{Er}^{L},

Table 1 Summary of the photophysical and chiroptical results of the four complexes studied, as well as the previously published [Er(*i*PrPyBox-NMe$_2$)$_2$]·3OTf complex

Complex	ε/M^{-1} cm^{-1} (λ/nm)	τ_{obs}/μs	Q^{L}_{Er} (%)	Q^{Er}_{Er} (%)	η_{sens} (%)	$\lvert g_{lum}\rvert$ (λ/nm)	B_{CPL}/M^{-1} cm^{-1}
CsEr(hfbc)$_4$	34 830 (311)	6.6	0.004	0.07	6	0.83 (1510)	0.23[a]
[TMG−H$^+$]$_3$Er(BINOLate)$_3$	59 279 (335)	0.4	0.0002	0.01	5	0.29 (1545)	0.0005[a]
Er(NTA)$_3$PhPyBox	42 752 (335)	2.7	0.003	0.03	10	0.06 (1523)	0.035[a]
Er(NTA)$_3$*i*PrPyBox	10 246 (367)	2.7	0.003	0.03	10	—	—
[Er(*i*PrPyBox-NMe$_2$)$_2$]·3OTf[b]	59 586 (447)	4.0	0.03	0.04	75	0.33 (1539)	0.7

[a] Calculated using a modified formula (eqn S3, ESI). [b] See ref. [1].

for the extended ethynyl-PyBox Er complexes recently reported by us (Table 1).[1] This highlights the importance of the tailored antenna ligand with suitable donor states in order to efficiently sensitise the low-lying Er emissive levels. On the other hand, the particularly high τ_{obs} of CsEr(hfbc)$_4$ indicates a relatively reduced multiphonon quenching by ligand vibrational overtones. A higher sensitisation efficiency (10%) is obtained in the case of Er(NTA)$_3$*i*Pr/PhPyBox complexes. The observed emission lifetime is approximately double with respect to optically inactive Er diketonates.[47,55] Finally [TMG−H$^+$]$_3$Er(BINOLate)$_3$ compounds display the shortest τ_{obs} and the lowest Q^{L}_{Er} (0.0002%), in contrast with the closely related alkali metal Er BINOLate.[3] A possible explanation could lie in the multiphonon quenching by the guanidinium N–H low-frequency oscillators in proximity of the Er centre in [TMG−H$^+$]$_3$Er(BINOLate)$_3$ complexes.

Consistently with the Yb and Eu analogue,[2,12,42] CsEr(hfbc)$_4$ exhibits the highest $\lvert g_{lum}\rvert$ factors among the Er complexes discussed here. In particular, the 1510 nm value (0.83) is the highest value reported for Er CPL, to the best of our knowledge. Such a value represents a 70/30 ratio of the two circularly polarised components of the emission.

[TMG−H$^+$]$_3$Er(BINOLate)$_3$ displays $\lvert g_{lum}\rvert$ values in line with its alkali metal Er BINOLate analogue, in spite of a significantly different geometry.[3] Finally and remarkably, in the case of diketonate complexes, only Er(NTA)$_3$PhPyBox showed a significant chiroptical activity in the NIR-IR. This is at odds with the behaviour of Eu and Yb similar complexes, where the complexes bearing *i*PrPybox ligand displayed similar or higher CPL activity with respect to the PhPyBox counterpart.[25,26,48,50] This can be rationalised by considering that an emergent vanishing signal can be observed if transitions between M_J levels are very close in energy and bear an opposite sign. This is ultimately due to the crystal field splitting induced directly or indirectly by different ancillary ligands. To take into account all the different and independent parameters that contribute to an overall efficient CPL emitter, we recently devised the so-called CPL brightness (B_{CPL}).[56] [TMG−H$^+$]$_3$Er(BINOLate)$_3$ shows a very low B_{CPL}, one order of magnitude below that of Er(NTA)$_3$*i*PrPyBox. On the other hand, CsEr(hfbc)$_4$ shows the highest B_{CPL}, due to the high g_{lum} and reduced multiphonon quenching, as indicated by the relatively large τ_{obs} (Table 1).

In all cases, NIR-CD spectra are very similar to the corresponding NIR-CPL ones (Fig. S6, S12 and S18, ESI†). The similarities between the NIR-CD and CPL in Er complexes are consistent with our previous observations.[1] Such behaviour stems from the fact that M_J levels of the $^4I_{15/2}$ and $^4I_{13/2}$ terms are closely spaced in energy, so that they are significantly populated at room temperature (k_BT at 300 K is 209 cm^{-1}). This has the effect that, unlike with other lanthanides, most transitions of the $^4I_{15/2} \leftrightarrow {}^4I_{13/2}$ manifold are observed both in absorption and emission and with a similar rotatory strength.[1] Note that the solutions used for NIR emission/CPL spectra have a very low optical density ($A < 10^{-3}$), thus excluding self-absorption contributions to NIR-CPL spectra.

Conclusions

We have shown that, despite low emission efficiency, NIR-CPL in the 1400–1600 nm range can be easily achieved with relatively simple Er chiral complexes, both homo- and heteroleptic ones. In particular, hfbc ligand proves its remarkable ability to induce strong CPL onto lanthanide complexes, even in the NIR region. Moreover, we have shown that the experimental setup for measuring NIR-CPL, which utilises inexpensive optics adapted for commercially available fluorimeters through suitable 3D-printed holders, produces reliable and repeatable results which otherwise could not be achieved by any instrumentation currently commercially available. A wider accessibility of suitable complexes and measuring capabilities will hopefully open the way to novel applications of NIR-CPL emitters for bioassays and NIR CP-OLEDs.

Author contributions

O.G.W. carried out spectroscopic measurements, data analysis and complex synthesis; A.P. gave instrumentation support; E.C. supervised lifetime measurements; F.Z. and L.D.B. conceived the idea, supervised the whole work, and discussed the data regularly; O.G.W. and F.Z. wrote the manuscript. All authors read and approved the final manuscript.

Conflicts of interest

There are no conflicts to declare.

Acknowledgements

O.G.W. is grateful for the financial support from the European Commission Research Executive Agency, Horizon 2020 Research and Innovation Programme under the Marie Sklodowska-Curie

grant agreement No. 859752-HEL4CHIROLED-H2020-MSCA-ITN-2019. This project has also received funding from the Italian Ministero dell'Università, PRIN 20172M3K5N. F.Z. and A.P. acknowledge financial support from the University of Pisa (PRA 2020_21).

References

1 O. G. Willis, F. Petri, G. Pescitelli, A. Pucci, E. Cavalli, A. Mandoli, F. Zinna and L. Di Bari, *Angew. Chem., Int. Ed.*, 2022, **61**, e202208326.
2 O. G. Willis, F. Zinna, G. Pescitelli, C. Micheletti and L. Di Bari, *Dalton Trans.*, 2022, **51**, 518–523.
3 N. F. M. Mukthar, N. D. Schley and G. Ung, *J. Am. Chem. Soc.*, 2022, **144**, 6148–6153.
4 M. Deng, N. D. Schley and G. Ung, *Chem. Commun.*, 2020, **56**, 14813–14816.
5 L. Arrico, C. Benetti and L. Di Bari, *ChemPhotoChem*, 2021, **5**, 815–821.
6 P. Stachelek, L. MacKenzie, D. Parker and R. Pal, *Nat. Commun.*, 2022, **13**, 553.
7 C. Lincheneau, C. Destribats, D. E. Barry, J. A. Kitchen, R. D. Peacock and T. Gunnlaugsson, *Dalton Trans.*, 2011, **40**, 12056–12059.
8 D. E. Barry, J. A. Kitchen, L. Mercs, R. D. Peacock, M. Albrecht and T. Gunnlaugsson, *Dalton Trans.*, 2019, **48**, 11317–11325.
9 M. Starck, L. E. MacKenzie, A. S. Batsanov, D. Parker and R. Pal, *Chem. Commun.*, 2019, **55**, 14115–14118.
10 D. E. Barry, D. F. Caffrey and T. Gunnlaugsson, *Chem. Soc. Rev.*, 2016, **45**, 3244–3274.
11 A. T. Frawley, R. Pal and D. Parker, *Chem. Commun.*, 2016, **52**, 13349–13352.
12 J. L. Lunkley, D. Shirotani, K. Yamanari, S. Kaizaki and G. Muller, *J. Am. Chem. Soc.*, 2008, **130**, 13814–13815.
13 H.-Y. Wong, W.-S. Lo, K.-H. Yim and G.-L. Law, *Chemistry*, 2019, **5**, 3058–3095.
14 F. Zinna and L. Di Bari, *Chirality*, 2015, **27**, 1–13.
15 L. E. MacKenzie and R. Pal, *Nat. Rev. Chem.*, 2021, **5**, 109–124.
16 B.-A. N. Willis, D. Schnable, N. D. Schley and G. Ung, *J. Am. Chem. Soc.*, 2022, **144**, 22421–22425.
17 F. Zinna, U. Giovanella and L. D. Bari, *Adv. Mater.*, 2015, **27**, 1791–1795.
18 Y. Yang, R. C. da Costa, D.-M. Smilgies, A. J. Campbell and M. J. Fuchter, *Adv. Mater.*, 2013, **25**, 2624–2628.
19 J. R. Brandt, F. Salerno and M. J. Fuchter, *Nat. Rev. Chem.*, 2017, **1**, 0045.
20 B. L. Feringa, *Acc. Chem. Res.*, 2001, **34**, 504–513.
21 R. Farshchi, M. Ramsteiner, J. Herfort, A. Tahraoui and H. T. Grahn, *Appl. Phys. Lett.*, 2011, **98**, 162508.
22 R. Carr, N. H. Evans and D. Parker, *Chem. Soc. Rev.*, 2012, **41**, 7673–7686.
23 M. Leonzio, A. Melchior, G. Faura, M. Tolazzi, M. Bettinelli, F. Zinna, L. Arrico, L. Di Bari and F. Piccinelli, *New J. Chem.*, 2018, **42**, 7931–7939.
24 J. Yuasa, T. Ohno, H. Tsumatori, R. Shiba, H. Kamikubo, M. Kataoka, Y. Hasegawa and T. Kawai, *Chem. Commun.*, 2013, **49**, 4604–4606.
25 F. Zinna, L. Arrico, T. Funaioli, L. Di Bari, M. Pasini, C. Botta and U. Giovanella, *J. Mater. Chem. C*, 2022, **10**, 463–468.
26 F. Zinna, L. Arrico and L. Di Bari, *Chem. Commun.*, 2019, **55**, 6607–6609.
27 S. Yamashita, *IEEE J. Sel. Top. Quantum Electron.*, 2001, **7**, 41–43.
28 C.-H. Yeh, C.-C. Lee and S. Chi, *IEEE Photonics Technol. Lett.*, 2003, **15**, 1053–1054.
29 C. L. Maupin, D. Parker, J. A. G. Williams and J. P. Riehl, *J. Am. Chem. Soc.*, 1998, **120**, 10563–10564.
30 C. L. Maupin, R. S. Dickins, L. G. Govenlock, C. E. Mathieu, D. Parker, J. A. G. Williams and J. P. Riehl, *J. Phys. Chem. A*, 2000, **104**, 6709–6717.
31 B. Lefeuvre, C. A. Mattei, J. F. Gonzalez, F. Gendron, V. Dorcet, F. Riobé, C. Lalli, B. Le Guennic, O. Cador, O. Maury, S. Guy, A. Bensalah-Ledoux, B. Baguenard and F. Pointillart, *Chem. – Eur. J.*, 2021, **27**, 7362–7366.
32 E. Cavalli, C. Nardon, O. G. Willis, F. Zinna, L. Di Bari, S. Mizzoni, S. Ruggieri, S. C. Gaglio, M. Perduca, C. Zaccone, A. Romeo and F. Piccinelli, *Chem. – Eur. J.*, 2022, **28**, e202200574.
33 R. S. Dickins, J. A. K. Howard, C. L. Maupin, J. M. Moloney, D. Parker, J. P. Riehl, G. Siligardi and J. A. G. Williams, *Chem. – Eur. J.*, 1999, **5**, 1095–1105.
34 F. Gendron, S. Di Pietro, L. Abad Galán, F. Riobé, V. Placide, L. Guy, F. Zinna, L. Di Bari, A. Bensalah-Ledoux, Y. Guyot, G. Pilet, F. Pointillart, B. Baguenard, S. Guy, O. Cador, O. Maury and B. Le Guennic, *Inorg. Chem. Front.*, 2021, **8**, 914–926.
35 F. S. Richardson, *Inorg. Chem.*, 1980, **19**, 2806–2812.
36 J. Li, C. Hou, C. Huang, S. Xu, X. Peng, Q. Qi, W.-Y. Lai and W. Huang, *Research*, 2020, 3839160.
37 E. M. Sánchez-Carnerero, A. R. Agarrabeitia, F. Moreno, B. L. Maroto, G. Muller, M. J. Ortiz and S. de la Moya, *Chem. – Eur. J.*, 2015, **21**, 13488–13500.
38 K. Ma, W. Chen, T. Jiao, X. Jin, Y. Sang, D. Yang, J. Zhou, M. Liu and P. Duan, *Chem. Sci.*, 2019, **10**, 6821–6827.
39 H. Tanaka, Y. Inoue and T. Mori, *ChemPhotoChem*, 2018, **2**, 386–402.
40 Y. Nagata and T. Mori, *Front. Chem.*, 2020, **8**, 1–6.
41 D. Shirotani, H. Sato, K. Yamanari and S. Kaizaki, *Dalton Trans.*, 2012, **41**, 10557–10567.
42 J. L. Lunkley, D. Shirotani, K. Yamanari, S. Kaizaki and G. Muller, *Inorg. Chem.*, 2011, **50**, 12724–12732.
43 S. Di Pietro and L. Di Bari, *Inorg. Chem.*, 2012, **51**, 12007–12014.
44 J. R. Robinson, X. Fan, J. Yadav, P. J. Carroll, A. J. Wooten, M. A. Pericàs, E. J. Schelter and P. J. Walsh, *J. Am. Chem. Soc.*, 2014, **136**, 8034–8041.
45 H. Sasai, T. Suzuki, S. Arai, T. Arai and M. Shibasaki, *J. Am. Chem. Soc.*, 1992, **114**, 4418–4420.
46 L. Di Bari, M. Lelli, G. Pintacuda, G. Pescitelli, F. Marchetti and P. Salvadori, *J. Am. Chem. Soc.*, 2003, **125**, 5549–5558.
47 P. Martín-Ramos, I. R. Martín, F. Lahoz, S. Hernández-Navarro, P. S. Pereira da Silva, I. Hernández, V. Lavín and M. Ramos Silva, *J. Alloys Compd.*, 2015, **619**, 553–559.

48 J. Yuasa, T. Ohno, K. Miyata, H. Tsumatori, Y. Hasegawa and T. Kawai, *J. Am. Chem. Soc.*, 2011, **133**, 9892–9902.
49 L. Armelao, D. B. Dell'Amico, L. Bellucci, G. Bottaro, L. Di Bari, L. Labella, F. Marchetti, S. Samaritani and F. Zinna, *Inorg. Chem.*, 2017, **56**, 7010–7018.
50 M. Górecki, L. Carpita, L. Arrico, F. Zinna and L. Di Bari, *Dalton Trans.*, 2018, **47**, 7166–7177.
51 S. Meshkova, Z. Topilova, D. Bolshoy, S. Beltyukova, M. Tsvirko and V. Venchikov, *Acta Phys. Pol., A*, 1999, **95**, 983–990.
52 S. W. Magennis, A. J. Ferguson, T. Bryden, T. S. Jones, A. Beeby and I. D. W. Samuel, *Synth. Met.*, 2003, **138**, 463–469.
53 Q. Sun, P. Yan, W. Niu, W. Chu, X. Yao, G. An and G. Li, *RSC Adv.*, 2015, **5**, 65856–65861.
54 G. Mancino, A. J. Ferguson, A. Beeby, N. J. Long and T. S. Jones, *J. Am. Chem. Soc.*, 2005, **127**, 524–525.
55 S. I. Klink, L. Grave, D. N. Reinhoudt, F. C. J. M. van Veggel, M. H. V. Werts, F. A. J. Geurts and J. W. Hofstraat, *J. Phys. Chem. A*, 2000, **104**, 5457–5468.
56 L. Arrico, L. Di Bari and F. Zinna, *Chem. – Eur. J.*, 2021, **27**, 2920–2934.

